CHALMERS
UNIVERSITY OF TECHNOLOGY

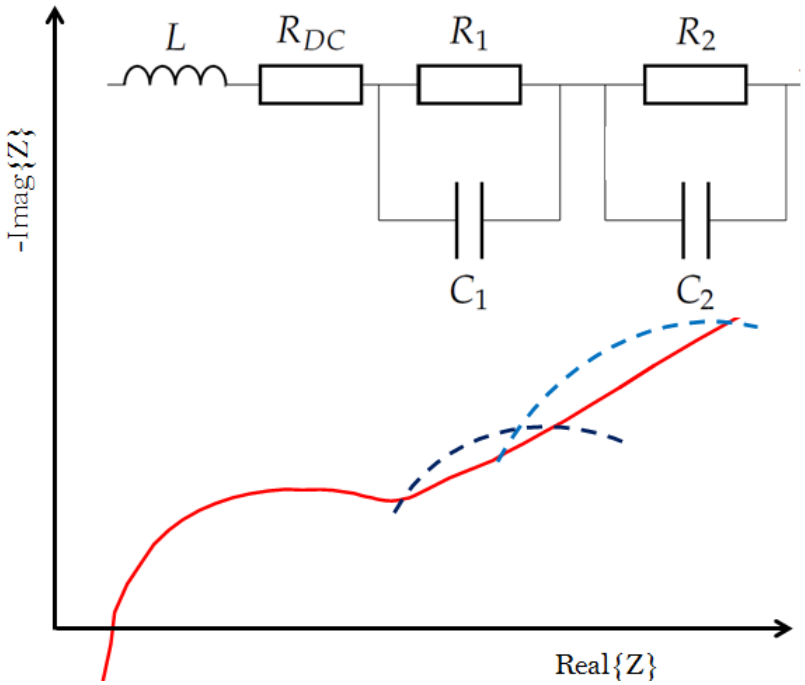

Pulse power characterisation for lithium ion cells in automotive applications

Small and large signal cell impedance analysis

Master's thesis in Electric Power Engineering

SANDEEP NITAL DAVID

Department of Energy and Environment
CHALMERS UNIVERSITY OF TECHNOLOGY
Gothenburg, Sweden 2016

MASTER'S THESIS REPORT 2016

Pulse power characterisation for lithium ion cells in automotive applications

Small and large signal cell impedance analysis

SANDEEP NITAL DAVID

CHALMERS
UNIVERSITY OF TECHNOLOGY

Department of Energy and Environment
Division of Electric Power Engineering
CHALMERS UNIVERSITY OF TECHNOLOGY
Gothenburg, Sweden 2016

Pulse power characterisation for lithium ion cells in automotive applications
Small and large signal cell impedance analysis
SANDEEP NITAL DAVID

Supervisors: Stefan Skoog, Chalmers
Bengt Axelsson, CEVT AB
Examiner: Torbjörn Thiringer, Energy and Environment

Department of Energy and Environment
Division of Electric Power Engineering
Chalmers University of Technology
SE-412 96 Gothenburg
Telephone +46 31 772 1000

Cover: Equivalent circuit model to represent EIS data in time domain

Typeset in LaTeX
Chalmers Bibliotek, Reproservice
Gothenburg, Sweden 2016

Pulse power characterisation for lithium ion cells in automotive applications
Small and large signal cell impedance analysis
SANDEEP NITAL DAVID
Department of Energy and Environment
Division of Electric Power Engineering
Chalmers University of Technology

Abstract

The pulse power capability of a Lithium ion cell is an important factor to be considered while dimensioning a traction battery pack. Pulse Power characterization of a Lithium ion cell requires an accurate Equivalent Circuit Model(ECM) in order to describe its dynamic behaviour. The two widely adopted methods for parametrising ECMs are the Current Interruption and Electrochemical Impedance Spectroscopy(EIS) methods. These methods are rarely unified for model development, and therefore this thesis seeks to analyse cells from two different chemistries using both methods in order to draw vital deductions regarding cell impedance behaviour under different operating conditions. The parametrised model obtained is validated using a vehicle driving cycle and a deviation of 30 mV in Root Mean Square Error(RMSE) value between measurement and simulation is obtained. The cell parameters are further used to derive and quantify the pulse power capability of a battery pack which consists of the cells used in this study.

Keywords: Lithium ion cell, Electrochemical Impedance Spectroscopy (EIS), Equivalent Circuit Modelling (ECM), Dual Polarisation (DP) model, Current Interruption (CI) method, Pulse power

Acknowledgements

First and foremost I would like to express my appreciation to my supervisor at Chalmers, Stefan Skoog, for his overwhelming technical support and guidance throughout this thesis. I also want to thank my supervisor at CEVT, Bengt Axelsson for providing the opportunity for this thesis and his constant support during the work. Furthermore, I would like to express my gratitude to my examiner, Torbjörn Thiringer, for all the meetings and insightful feedback on my practical and written work.

Sandeep David, Gothenburg, June 2016

Contents

List of Symbols and Abbreviations

HEV	Electric Vehicle
EV	Electric Vehicle
CI	Current Interruption
EIS	Electrochemical Impedance Spectroscopy
BT	Battery Tester
R_{DC}	Resistance of a cell within few hundred milliseconds
R_o	Cell ohmic resistance
CPE	Constant Phase Element
OCV	Open Circuit Voltage
SOC	State of Charge
ECM	Equivalent Circuit Model
TEM	Thermo Electric Module
C-rate	Current-rate
DP	Dual Polarization
Li	Lithium ion
SSE	Sum of Squared Errors
RMSE	Root Mean Square Error

Chapter 1

Introduction

1.1 Background

Dimensioning the traction battery pack for any form of hybrid or pure electric vehicle needs to encompass several parameters so that the vehicle is capable of meeting all its necessary performance criteria. When choosing cells for the battery pack, a factor which in general tends to be crucial is the maximum power extractable from the cells, or in short, the pulse power characteristic of a cell. This characteristic shows a strong dependency on the cell's impedance behaviour[1]. Moreover during high current loading, the heat generated from the battery and its energy efficiency are also primarily determined by the cell's internal impedance. Therefore the knowledge of the internal impedance of a lithium ion cell is one of the most important factors while designing a complete battery system. Investigations described in literature regarding cell impedance characteristics show that it depends on several factors which include the SOC, temperature, current magnitude and history of usage[1].

Two techniques which are predominantly used for cell impedance study are the Current pulse method and Electrochemical Impedance Spectroscopy. The former involves the measurement of the cell voltage response during or after a DC current pulse and concerns a study in the time domain[2], whereas the latter in comparison uses much smaller current signals and is a frequency domain study[3]. Therefore these two techniques will from now on be referred to as the Large signal and Small signal methods. These methods are rarely unified for model development and parametrisation, thus providing a niche for a significant research contribution through this thesis.

1.2 Aim

To quantify and validate the pulse power deliverable from a lithium ion cell through extensive investigation of its internal impedance at different operating SOCs, temperatures and current magnitudes. To also establish and validate a

suitable approach for modelling EIS measurements in the time domain.

1.3 Scope

This thesis is aimed at developing an accurate equivalent circuit model for a lithium ion cell by investigating its impedance characteristic under various operating conditions. The variations under which the cell impedance is studied includes different SOC points, temperatures and current magnitudes. The parameters for the ECMs are independently obtained through the Large and Small signal methods. Though presently a clear method for unifying the results from the two methods doesn't exist, this work will seek to make a contribution towards this. The parametrised ECMs obtained through each method will be verified, and followingly validated using the HPPC dynamic drive cycle. The results obtained will be further used for determining the pulse power limits of a cell. In order to further ascertain the results purported from this work, experiments will not be restricted to a single cell, but rather to three cells, covering two different chemistries which currently finds wide application in the automotive industry[4].

In practice, the pulse power deliverable by a cell also depends on the contribution it would have on the rapid aging of the cell. In other words, the maximum extractable power must be limited in order to conserve the life time of the cell. Numerous tests described in research publications show that high current discharge rates results in a much shorter cell life expectancy[5]. Studying the effect of discharge rates on cell aging requires numerous accelerated cycling tests to be performed on the cells and due to the limited time available, no such experiments on cell aging will be conducted during this thesis. Since the implications of higher discharge rates on cell-life span is quite evident, the pulse discharge current ratings explicitly specified by the cell manufacturer will be strictly adhered to throughout this thesis. Moreover since the temperature and voltage limits could also have a considerable impact of cell aging[6][7], these too will be adhered due to during all experiments.

This thesis is solely focused on the pulse discharge characteristics of cells and therefore studying the pulse charge characteristics is outside the scope. Moreover when considering cell performance modelling, any phenomena showing up at battery pack level which may include cell voltage imbalance, the BMS, cable inductance, HV connector resistance, fuse non-linearity, cell tab interconnection losses, etc. will not be taken into account.

1.4 Contributions

The highlight of this thesis is the possible unification of the Large and Small signal methods, and in doing so, being able to draw vital deductions from the data obtained from both backgrounds. This could lead to the developments of more comprehensive lithium ion cell models. Several researchers have used either method for measurements independently, but very few have used both simultaneously to enhance model development. Whilst trying to replicate EIS measurements in the frequency domain with their ECM models, researchers generally tend to use Constant Phase Elements(CPE)[5][8][9]. However, there is no accurate representation of CPEs in the time domain and therefore most researchers using the EIS technique find it hard to interpret their results, especially at lower frequencies(typically < 0.5 Hz). However understanding the cell behaviour from EIS measurement at lower frequencies is extremely important, especially while simulating automotive drive cycles[10].

In [11] Buller states that CPEs can be represented as an approximation in the time domain. The authors of [3] have made a suitable approximation for the CPEs in the time domain which gave satisfactory results but use as many as 3 RC networks which can be considered as fairly complex in terms of computational power required for its real-time implementation. Hereby this work will focus on trying to further simplify the complexity of the ECMs required to approximate the EIS data from the frequency domain to the time domain. During this work several ECMs ranging from being highly accurate yet complex, to less accurate and simple models will be devised to represent EIS data for different cells at different SOCs and temperatures in the time domain. The results obtained from these ECMs will be both verified and validated appropriately. They will then be used to derive the cell's pulse power limits at various conditions. During the course of this work, some characteristic trends observed in terms of cell behaviour with respect to type of cell chemistry or operating conditions will be mentioned, and further substantiated with previously published research work.

1.5 Thesis outline

Following a brief introduction for the thesis covered in this chapter, a comprehensive collection of used theory with respect to equivalent circuit modelling in the time and frequency domain is presented in the chapters to follow. Consequently the test setups for all the experiments conducted are described together with visualisations for some of the important measurements obtained. Model fitting of the practical data in both time and frequency domain are comprehensively analysed, followed by their verification and validation explained in independent chapters. In conclusion, pulse power limits for the cells are derived and then the thesis is concluded with some inferences obtained together with comments on future work which could be done.

Chapter 2

Equivalent circuit modelling: Time domain

2.1 Cell chemistries under consideration

Two different cell chemistries are used for experiments during this work. This section provides a brief summary for each chemistry used, in addition to highlighting its intrinsic characteristics.

Lithium Nickel Manganese Cobalt Oxide (NMC): This cell type combines a nickel cathode which has high specific energy, together with a manganese structure which gives it a very low internal resistance. It is commonly used together with a graphite anode. These cells typically have a nominal cell voltage of around 3.65 V and a maximum voltage of 4.2 V. NMC type cells have potentially long cycle lives and good characteristics with respect to safety. These cells can be customized by the manufacturer to have high specific energy or high specific power[12].

Lithium Iron Phosphate (LFP): When LFP is used as a the cathode material, it has becomes very safe, has good thermal stability, high tolerance to abuse, high power density and long cycle life. It is commonly used together with a graphite anode. However its energy density is relatively lower than other mixed metal oxides. This can be mainly attributed to the fact that it has a lower nominal cell voltage of 3.3V and maximum of 3.6V. Notably LFP has a higher self-discharge than other Li-ion batteries[12].

2.2 Cell impedance phenomena to be observed

Cell impedance can be described in terms of the voltage drop over a cell when a load current is applied as shown in Figure 2.1. In the first moment after applying the current pulse, the voltage drops immediately over its pure ohmic resistance, followed by the charge transfer resistance within a few hundred milliseconds.

The gradual voltage decrease measured further on in time is mainly due to the slow diffusion processes taking place within the cell. Likewise when the current stops flowing, the ohmic voltage drop immediately disappears followed quickly by the disappearance of the voltage drop due to the charge transfer resistance. The slow rise observed thereafter in the voltage curve is again due to slow diffusion processes taking place.

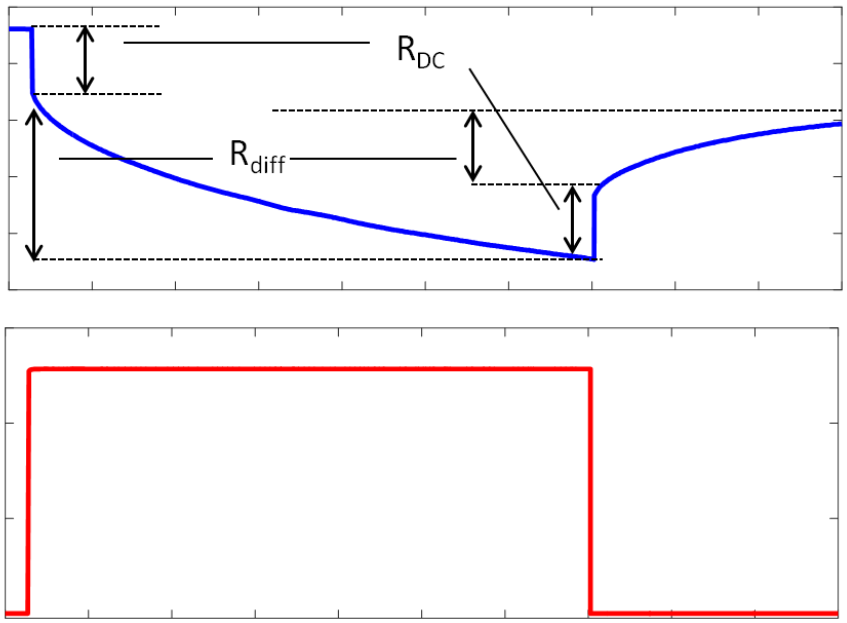

Figure 2.1: Voltage drop over cell upon discharge current pulse

2.2.1 Cell Open Circuit Voltage

The difference between the two electrodes of a cell at zero current density is called the open circuit voltage of the cell at a given state-of-charge. According to the work in [13], the OCV predominantly varies with SOC and is typically found to be fairly independent of temperature between the range of -10 to 50°C.

2.2.2 DC Resistance

The term DC Resistance R_{DC} is used to refer to the voltage drop which occurs across the cell from the instant of applying a current pulse till the first few hundreds of milliseconds. Therefore it comprises of not only the ohmic voltage drop but also the voltage drop due to charge transfer polarisation.

2.2.2.1 Ohmic voltage drop

This voltage drop is a combination of the resistances arising from the active material of the anode and the cathode, the separator and the electrolyte[14].

2.2.2.2 Charge transfer polarisation

This time-dependent resistance is attributed to the double layer capacitance which occurs between the electrolyte and the ions traveling through the electrolyte towards the anode or cathode. The charge transfer resistance reflects the charge-transfer process during the reactions taking place on the electrode–electrolyte interfaces.

2.2.3 Diffusion polarisation

This is the main factor contributing to the sluggish voltage response of the cell both during and after a current pulse. The Li ions need to be transported from the surface to the centre of the active material, and this process is termed as solid state diffusion. The concentration difference between the Li concentration at the surface, and the equilibrium concentration causes the diffusion polarisation[15].

2.3 Choice of method for cell parametrisation

2.3.1 Overview of common techniques used

The authors in [16] have discussed several methods for determining the internal impedance of a cell. Two general methods discussed either involved using current steps to study the voltage response or measuring the heat loss from the cell. Interestingly, both types of methods yielded same results. However, the current step method is used in this work as it more prevalent among researchers and also convenient since the accurate measurement of heat loss requires sophisticated equipment. While considering the current step method, one can either chose the current injection technique or the current interruption technique. Procedures involving both these methods were adopted in [2] and it is concluded that they give similar results provided that sufficient relaxation time is allowed while using the current interruption method. This is mainly to allow sufficient time for diffusion polarization to take place.

2.3.2 Current Interruption technique

The current interruption technique is utilised in this work for large signal based impedance analysis. This is mainly due to the fact that when current injection is performed, the SOC of the cell is no longer constant and therefore the extracted parameters cannot be associated with a specific SOC point. However, in accordance with[2], when using current interruption, sufficient time is allowed to account for diffusion polarisation. All experiments are done using discharge current pulses, thereby only determining the cell's discharge resistance, and not its charge resistance. Several researchers[17][18] have experimentally proven that charge and discharge resistances are certainly within comparable range, but typically show differing trends over the SOC range. Therefore it is evident that assuming identical values for charge and discharge resistance at the same operating

conditions would not lead to large inaccuracies in the models developed using them.

2.4 Model Selection

In order to predict the performance of a cell at different operating conditions and loading, simulations based on an ECMs are widely used[19][20][21]. ECMs which are used to represent battery dynamics are computationally more efficient than complex physical battery models and therefore well suited to applications in the BMS for EVs and HEVs. They are commonly used for two purposes: to predict battery performance and for accurate SOC prediction.

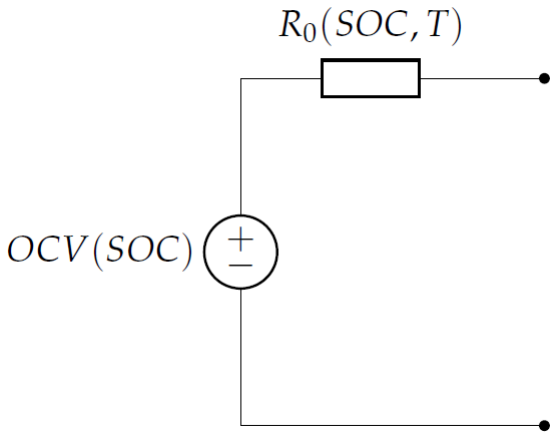

Figure 2.2: Rint model

The simplest ECM described in [22] is the Rint model shown in Figure 2.2. This model uses only two elements, representing the cell's OCV and its internal resistance respectively. The OCV is generally expressed as a function of SOC and resistance as function of SOC and temperature. However it is fairly obvious that this model will not be able to replicate the transient voltage behaviour which is typically exhibited by a Li-ion cell. Therefore one ought to incorporate a certain number of RC branches into this model in order to improve its modelling accuracy.

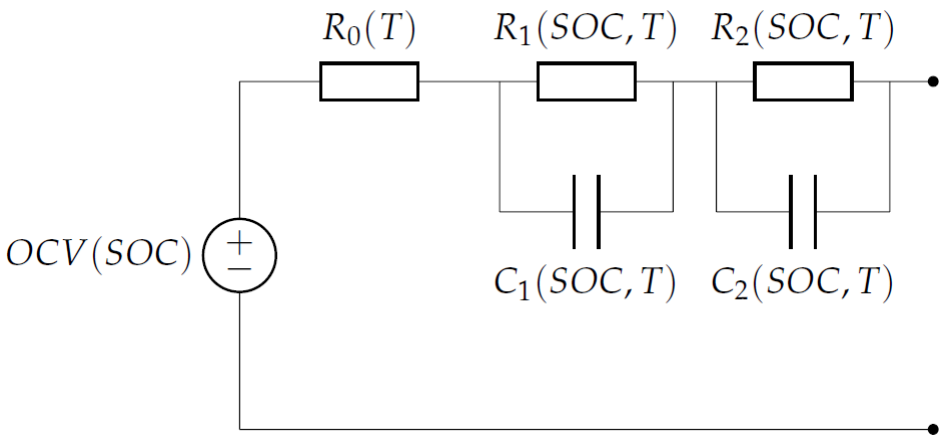

Figure 2.3: Dual Polarisation Model

The work in [20] shows that 3 RC branches are required in order to accurately capture both the quick and slow aspects of the transient behaviour of an LFP cell. However the issue with using 3 RC branches is the increased computational complexity involved and therefore a slightly simpler option is sought for. The authors of[19] and [22]have compared simpler models which include the Dual Polarisation(DP),Single Polarisation(SP) model and the Rint model. These models have two, one and no RC branches respectively. Results from these works show that the DP model shown in Figure 2.3 achieves a good compromise between model accuracy and complexity, wherein one RC branch represents the quick transient while the other represents the relatively slower transient.

Based on these mentioned findings, the DP model is chosen as the candidate to analyse cell impedance behaviour under various operating conditions. Since the DP ECM will be used to replicate the cell's voltage rise after the current pulse has been removed,

$$V_t = V_0 + V_1 e^{-\frac{t}{R_1 C_1}} + V_2 e^{-\frac{t}{R_2 C_2}} \tag{2.1}$$

can be mathematically used to represent this type of behaviour. In fact, this equation forms the basis for the curve fitting tool which is to be used for parameter extraction.

Chapter 3

Equivalent circuit modelling: Frequency domain

3.1 EIS

EIS is a widely used technique to investigate electrochemical systems. It is especially valuable when used as a tool to calculate and observe various phenomena occurring within a cell. The advantage of EIS is that it is non-destructive to the investigated system. It basically involves imposing a small sinusoidal current signal at a given frequency on the cell. The voltage response measured at the cell is approximately a sinusoidal signal, and this procedure is repeated across a wide range of frequencies. Finally, the impedance Z of the system is calculated and expressed in terms of its real and imaginary magnitudes in milli-ohms as a function of the frequency. The phenomena arising at different regions in the frequency spectrum are thus obtained and some characteristic points can be used to describe the dynamic behavior of the cell, thereby allowing the creation of models.

Since the excitation signal used is sinusoidal, a significant consequence is that the cell being tested remains at the same SOC point throughout the entire EIS measurement. Also, unlike in the Large signal method, the impedance measured is neither the charge nor discharge impedance but rather the average of these two quantities.

3.2 Characteristic points on the EIS measurements

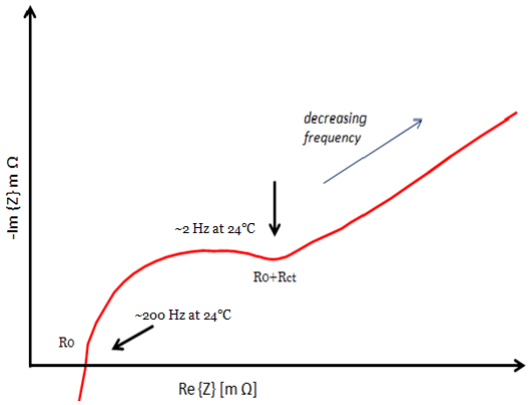

Figure 3.1: Typical EIS measurement at a specific SOC and Temperature

Upon analysing Figure 3.1, it can be inferred that at very high frequencies the spectrum shows inductive behaviour caused by metallic elements in the cell and cables. The curve's intersection with the real axis, approximately represents the ohmic resistance R_o which is the sum of the resistances of current collectors, active material, electrolyte and separator [5]. The semicircle-like shape which follows is typically associated with the double layer capacity and charge transfer resistance Rct at the electrodes. According to [5], the real part of the impedance at the local minima approximately represents the sum of R_o and R_{ct}. In older cells, a second semi circle might also be present, representing the SEI layer which is formed during cycling on the surface of the anode. The final, low frequency part of the curve is attributed to the diffusion processes taking place in the active material of the electrodes[21]. This low frequency diffusion gives rise to what is known as the Warburg impedance. At the initial part of the spectrum, i.e. at the high frequencies, the Warburg impedance isn't very significant since diffusing reactants don't have to move very far. However at low frequencies, the reactants have to diffuse farther, thus increasing the Warburg-impedance[23].

3.3 Model Selection

3.3.1 Equivalent circuit with Constant phase elements

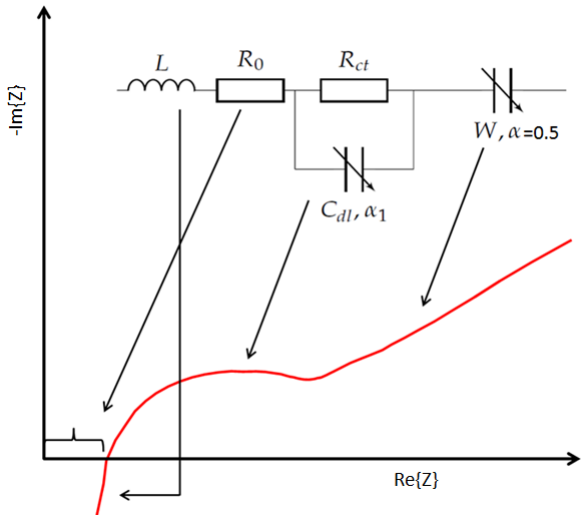

Figure 3.2: CPE based ECM representation of EIS data

Despite the fact that EIS can be used for comprehensively determining the cell impedance by distinguishing its individual components such as ohmic, charge transfer and mass transfer polarizations from a single experiment, it often faces the issue of being too complex, especially in terms of interpretation of the data. Using the data obtained from EIS measurements,appropriate ECMs are parametrised through fitting procedures in the frequency domain in order to be able to interpret the EIS results in the time domain.

The most common ECMs used for modelling EIS data comprise of constant phase elements, which are needed in order to obtain a satisfactory fit with the EIS measurements. Typical EIS measurements can be fitted by equivalent circuits as shown in Figure 3.2 which were used in [5][3][8]. In these types of ECMs, L represents the inductive behaviour at high frequencies, R_o is ohmic resistance comprising of the electrolyte, separator, and electrode resistance. R_{ct} and C_{dl} are charge-transfer resistance and its related double-layer the mid-frequency range. The Warburg impedance which is related to the diffusion of the lithium ions in the active material, is represented by a straight sloping line at the low frequency.

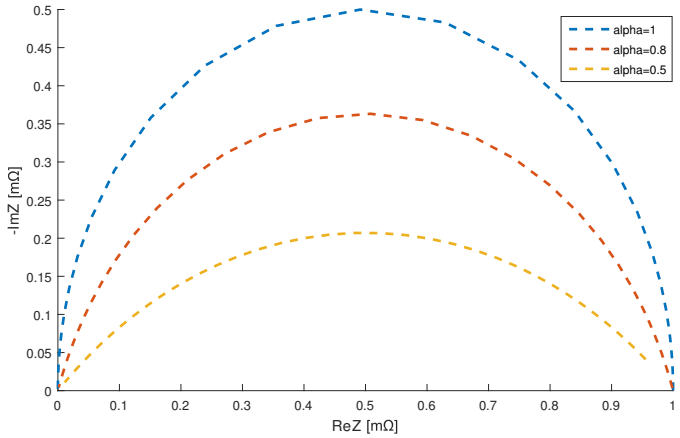

Figure 3.3: Impact of alpha value on CPE behaviour in frequency domain

In the mid-frequency range of the EIS measurement shown in Figure 3.1, it can be seen that the shape of the spectrum doesn't represent an ordinary semicircle, but rather a depressed semicircle. Using an ordinary capacitor to represent this kind of behaviour in the frequency domain is not successful since it is incapable of producing the depressed-circles. Capacitors show up at perfect half cycles when modelled in the frequency domain. Therefore, a CPE is necessary in order for the ECM to reproduce a depressed-circular shape in the frequency domain and is the reason why there are commonly used in ECMs to represent EIS data.

A CPE is a non-intuitive circuit element that is invented while looking at the response of real-world systems. The depressed semicircle which it exhibits in the frequency domain has been explained to be due to the fact that some property of the system is not homogeneous or that there is some distribution or dispersion of the value of some physical property of the system. A CPE can be mathematically represented as

$$Z_{CPE} = \frac{1}{(j\omega)^{\alpha}C} \tag{3.1}$$

where C is its capacitive impedance, ω is the frequency and α represents the ratio of the extent of its behaviour between a capacitor and resistor. The value of α controls the level of depression of the semicircles as is seen in Figure 3.3.

Similar to how the CPE is used to model C_{dl}, it is also used to represent the Warburg impedance. Since the Warburg impedance appears as a straight line with a slope at roughly 45°, it basically has almost equal real and imaginary impedances at the lower frequencies. Therefore it can be modelled as a CPE with a with α=45°. Once again the issue with using CPEs in the ECMs is that they have no physical representation and therefore it makes it hard to interpret the results obtained from these ECMs.

3.3.2 Equivalent circuit with RC elements

3.3.2.1 Comprehensive model:6 RC

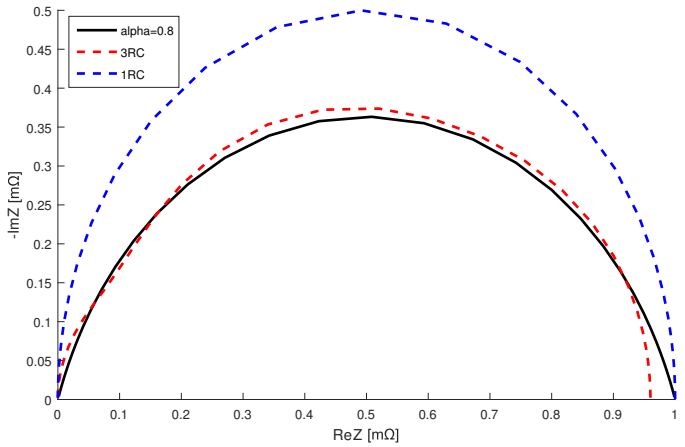

Figure 3.4: Approximate representation of CPE using RC elements

Buller in his work [11] found that it is possible to find approximations for a CPE using only R and C elements. He suggested both 5 RC and 3 RC based networks whose values when chosen suitably become equivalent to a CPE. The 5 RC model is more accurate but the 3 RC model is more computationally efficient since it involved lesser number of parameters. Buller also validated both models in his work and suggested that the 3 RC network is recommended as the general simulation tool and the fit it gives to replicate the behaviour of a CPE is shown in Figure 3.4.

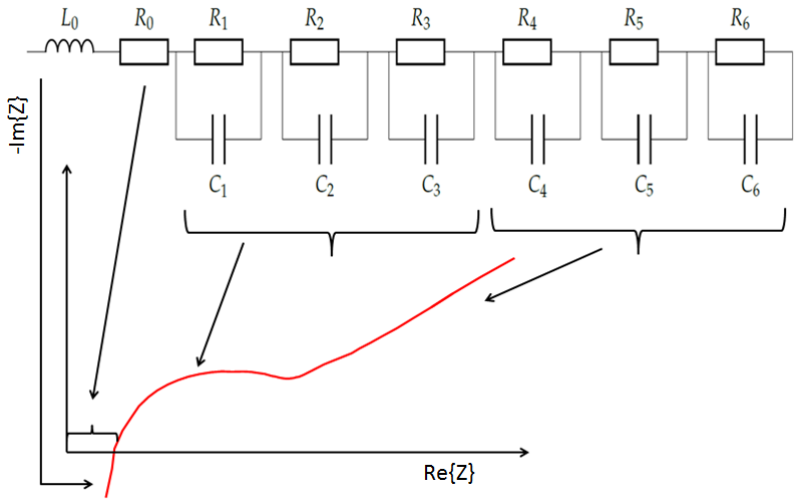

Figure 3.5: Comprehensive RC network based representation

Adopting the findings of Buller, the 3 RC nework is used to replace the 2 CPEs in the ECM depicted in Figure 3.2. Therefore a total of six RC elements were

required in the new ECM in Figure 3.5. Since the values of α are different for each of the two CPEs, they need to be represented independently with 3 RC networks. While performing the model fitting using numerical optimisation algorithms, a fit similar to that shown in Figure 3.4 can be expected.

3.3.2.2 Approximation based model:2 RC

As discussed in the previous section, the 6 RC model is able to comprehensively replicate the EIS measurements without any CPEs. However a 6 RC ECM is very complex and requires a lot of computational power. It is therefore not a practically viable option. In order to further simplify the 6 RC based ECM without sacrificing too much accuracy, a new 2 RC based model is proposed, wherein a fixed Resistance R_{DC} and 2 RC networks represent the EIS data. This ECM is depicted in Figure 3.6. It is evident that this ECM isn't capable of replicating the complete spectrum, but it can be made to replicate a certain aspect of the spectrum.

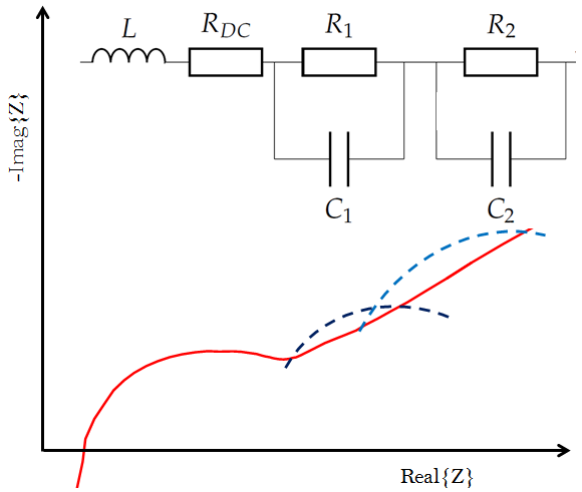

Figure 3.6: Approximate 2 RC network based representation

Considering the fact that this ECM is to be applied in an automotive application, where drive cycle frequencies are typically lower than 2 Hz, this model can be tuned to only focus on capturing the low frequency behaviour of the cell. The low frequency behaviour of the cell is basically governed by its diffusion processes, and therefore it is generally the Warburg impedance which needs to be captured by these two RC networks. According to this approach, R_{CT} is coupled with R_o and represented together as R_{DC} and so this model closely represents the DP model described in the previous chapter2.4. Even though this ECM fails to capture the time dynamic caused by C_{dl}, the typical values of C_{dl} found in other related works[8][24] and my work, are in the range of nearly 100F. This C_{dl} value when multiplied with R_{CT}, gives a maximum time constant of upto a couple hundreds of milliseconds. Since such high frequencies are not very relevant while running automotive drive cycle, its exclusion can be justified.

Chapter 4

Experimental setup and Measurements: Large signal

4.1 Test setup

Since this large signal test method utilises large current pulse magnitudes, it is necessary that all electrical connections are made appropriately in order to avoid unnecessary voltage drop which could lead to measurement inaccuracies. In order to achieve a good connection between the cables of the test equipment and the cell tabs, copper bars are used to provide a high clamping force. Additionally it is necessary to include sufficient insulation between the cell tabs in order to avoid the possibility of external short circuiting of the cell.

Table 4.1 shows a list of cells which are used during this work. Individual cells are been assigned unique tag names which are used to refer to them from here onwards.

Table 4.1: List of cells to be investigated

Cell tag	Cell name	Type	Package
Cell A	Cell 25Ah	NMC	Pouch
Cell B	Cell 30Ah	NMC	Pouch
Cell C	A123 19.5Ah	LFP	Pouch

4.1.1 Cell formatting

Before performing any kind of experiments on new or unused cells, they must be undergo "formatting" or "formation cycling" which is the process by which a cell is cycled multiple times consecutively using a moderately low current (typically 1C). The test protocols for formation cycling are similar to capacity tests which are designed to measure the maximum capacity that a cell can supply between two predefined voltage limits. The reason for performing the formation cycles is to gradually build up the film that forms on the surface of the electrodes known

as the solid-electrolyte inter-phase layer. This layer facilitates the flow of Li ions and prevents internal shorting, which could be otherwise caused by dendrite formation. Since Li-ions are consumed in this layer formation, it leads to initial irreversible capacity loss[5]. Constructing a stable and efficient SEI is among the most effective strategies to inhibit the dendrite growth and to thus achieve a superior cycling performance[25]. An ideal SEI is one which possesses minimum electrical conductivity and maximum Li + conductivity [25]. After formation, cells can undergo characterization tests and then the measurements obtained would be a better representation of the cell's long term behaviour.

4.2 Procedure

The general procedure for tests using the Digatron Battery Testing equipment involved studying how the cells behaviour over different SOCs at a particular temperature. The temperature is then changed and then the same procedure is repeated, according to the parameters stated in Table 4.2. Since the cells being tested are highly sensitive to temperature, it is necessary that the temperature is maintained constant throughout the test and for this a single NTC temperature sensor is used to monitor cell temperature. In order to maintain consistency in the procedure among all the tests on the different cells, a current magnitude of 2C is chosen as it is both high and within the limits of the equipment. For further clarification, when considering a 25 Ah cell, 2C would numerically mean a current of is 50 Amperes. A relaxation time of 60 minutes is allowed after every current pulse which is applied on the cell. The flowchart in Figure 4.1 briefly summarises the procedure followed during tests using the Digatron BT.

Table 4.2: List of parameter variations on Digatron tests

Parameter of interest	Test range	Other variables
State of Charge(SoC)	0 to 100 %	constant T, I=2C
Temperature	12 to 36 °C	0 to 100 %, I=2C
Current Magnitude	0.5C to 5C	T=24 °C, 0 to 100 % SOC

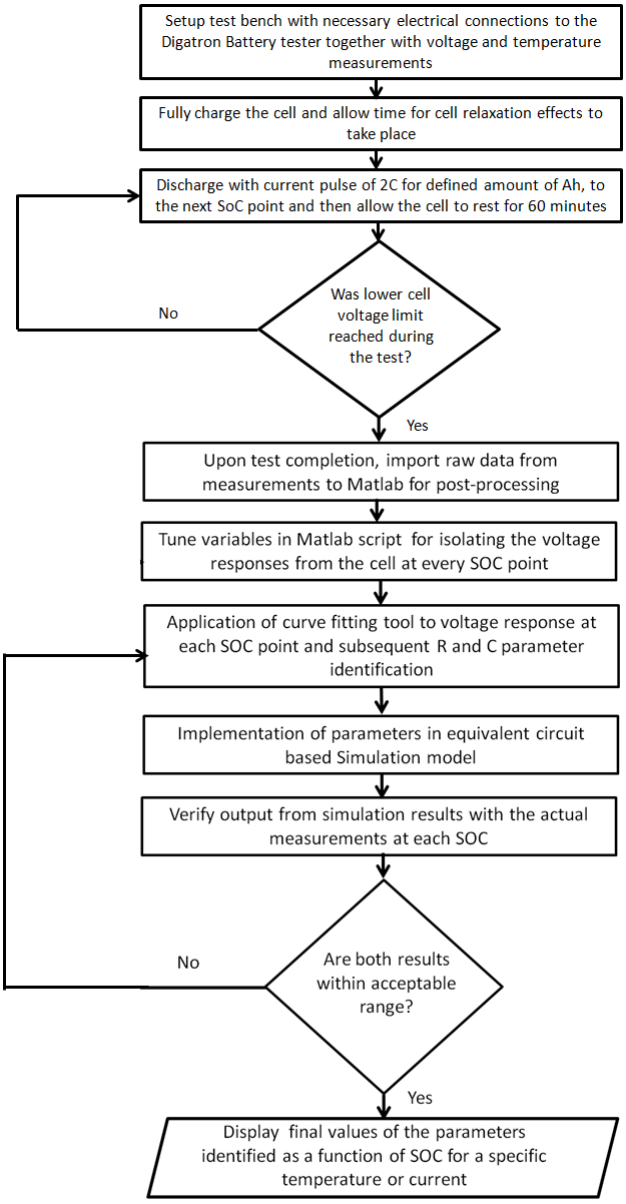

Figure 4.1: Digatron overall procedure

4.2.1 Post-processing

Upon completion of the current pulse tests, the measurement data from the tests is imported to Matlab in order to use it for cell parameter extraction. The post-processing therefore involved extraction of the cell's voltage response at every SOC point and subsequent CM parameter identification from it. The methods used for it will be explained more in detail in Chapter 6.

4.3 Measurements

4.3.1 OCV curve determination

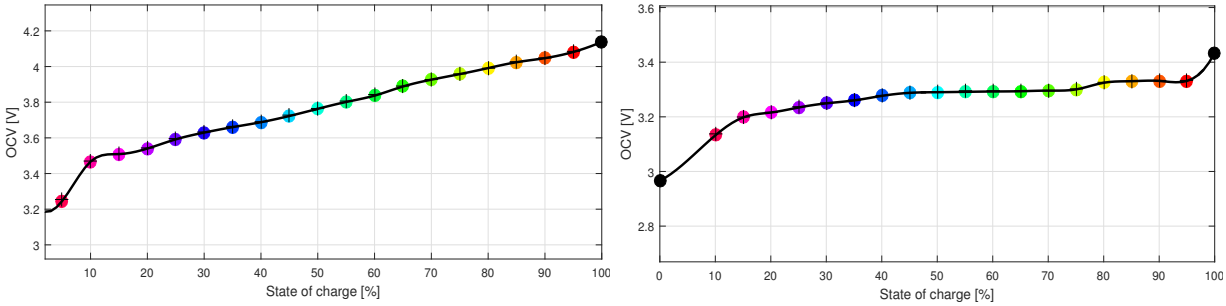

(a) OCV vs SOC for Cell A

(b) OCV vs SOC for Cell C

Figure 4.2: OCV curves for two different cell chemistries at 24 °C

Since cell parameters tend to show strong dependency on its operating SOC point, it is of utmost importance to experimentally determine the OCV characteristics for every cell which is under study using this large signal method. The principle used to determine the OCV at different points of the cell's SOC window involved measuring the cell's relaxed voltage after a current pulse has been applied. In other words, once a current pulse had been applied and the cell moved to a new SOC point, it is allowed to relax so that all the diffusion process had time to settle down and reach equilibrium. Ideally the cell should be relaxed for several hours for it to reach equilibrium. However in this procedure, only an hour is allowed for relaxation. Once this time had surpassed, and before the application of the next current pulse, the cell voltage is measured and recorded as its OCV at that particular SOC point. Since the cell isn't allowed to rest for a very long period of time, which is necessary for it to reach steady state, the OCV measured may be slightly inaccurate. To compensate for this, when the cell parameters are extracted and the ECM is developed, it is run with a similar current pulse and then its voltage response at nearly infinite time(or steady state) is considered as the OCV.

Figure 4.2 shows the plots for OCV vs SOC for cells A and C. It is evident that Cell A has a much sharper gradient in its OCV between its SOC limits, where Cell C has a much flatter voltage profile. This behaviour is due to the difference in the cell chemistries, and more specifically due to the phase transitions that take place within the cell. According to [26], the LFP cell chemistry inherently possesses a two-phase transition which results in a producing constant lithium concentrations within the phase regions and so shows only a minor change in OCV. On the contrary, cell A which is of NMC type chemistry has an OCV which drops by 0.6 V nearly linearly between its SOC limits due to the absence of the two phase transition effect.

4.3.2 Impedance behaviour over SOC

In order to comprehensively study the cell impedance behaviour over the operating SOC window of the cell, it is decided to use roughly 13-14 equally spaced SOC points. The intention is to maintain other factors which affect cell impedance constant, and to only focus the analysis on the impedance behaviour with respect to SOC. This experiment is done at room temperature and using current pulses of 2C. Relaxation time of up-to an hour is allowed so that the cell is almost completely rested by the time its voltage response is studied at the next SOC point. Typical measurements obtained from such a test as described above is shown in Figure 4.3

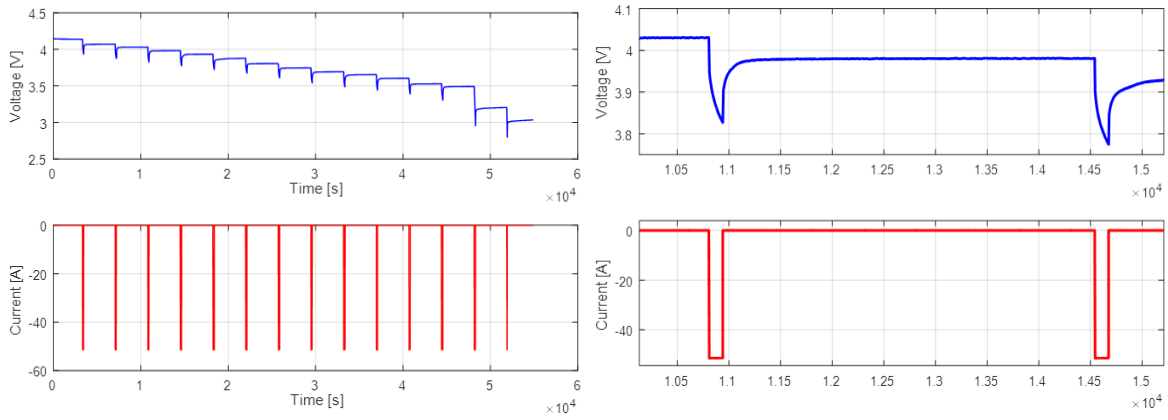

(a) **(b)**

Figure 4.3: Digatron voltage and current measurements for entire test 4.3a and magnified view for two pulses 4.3b

4.3.3 Impedance behaviour over temperature range

In order to study the effects of temperature on the cell impedance behaviour, this experiment is aimed at carrying out the exact procedure as is previously done to study the impedance behaviour over SOC. The difference in this case is that the cell is tested at different temperatures. The additional challenge in this experiment is trying to maintain the cell temperature at a constant value without using a climate chamber. This is accomplished by the use of Thermo Electric Modules(TEMs) which when suitably controlled are able to produce a heating or cooling effect on the cell being tested. However the temperature range under which the experiment could be conducted is limited by the capability of the TEMs to between 12 to 36 °C. Six modules are used to bring about the heating/cooling effect on the cell on one side of it. Since the system did not heat or cool both sides of the cell, it is necessary to use an additional temperature sensor to measure the temperature of the other side of the cell. It can be stated that an accuracy of $\pm 1°C$ is achieved in temperature measurement in this method.

4.3.4 Impedance behaviour with different current magnitudes

Since some parts of the cell's impedance seem to show strong dependency on the magnitude of current as suggested by the authors in [1], in addition to performing tests at different SOCs and temperatures, current pulses with different amplitudes are also applied for full characterisation of the cell impedance. Since applying high current magnitudes would result in extra cell heating, it is important to make sure that the cell's temperature is maintained constant under all loading conditions. The primary objective of this experiment is to isolate the effects of temperature on the cell's impedance, and to only obtain effect of the variation over C-rates. The climate chamber is used to conduct this test and suitable temperature measurements are in place. Additionally the cell being tested is sandwiched between two large metal bars in order to increase its thermal mass, and thereby reducing the opportunity for a rise in cell temperature during loading. C-rates used for this test ranged from 0.5C to 5C, while the temperature of the climate chamber is at 24 °C.

Chapter 5

Experimental setup and Measurements: Small signal

5.1 Test setup

EIS measurements on the selected cells were performed using a very sensitive scientific instrument, namely the GAMRY Reference 3000. The sine wave generator on this equipment allows its use for impedance measurements at a wide range of frequencies. It must be connected to a computer during its operation, and requires initial calibration before use to avoid effects of noise from the external environment. The Gamry is a four probe instrument and the functions of each of the probes required during the test is briefly described in the table below.

Table 5.1: Four wire connection for EIS measurement

Electrode name	Colour	Function
Working electrode	Green	Current-carrying from positive terminal
Counter	Red	Completes current path at negative electrode
Working sense	Blue	Voltage measurement at positive terminal
Reference	White	Voltage measurement at negative terminal

The instrument has three modes of operation. The Potentiostatic mode involves measuring the impedance by applying a sinusoidal voltage to the sample and measuring the current. The Galvanostatic EIS involves the application of an AC current and measurement of the potential. A galvanostatic EIS measurement provides higher accuracy and precision than potentiostatic EIS on low impedance samples such as batteries and fuel cells. This is because the potential can be measured with higher accuracy than it can be controlled. The Hybrid EIS mode is in essence a blend of potentiostatic and galvanostatic modes. It can be described as

a modified form of Galvanostatic EIS in which the applied AC current is continually adjusted to optimize the value of the measured potential[27].

The Hybrid EIS mode is found suitable to be used in the experiments throughout this work. Whilst setting up a Hybrid EIS measurement, the user specifies the desired AC Voltage, the estimated impedance of the sample and the frequency range. In the case, the magnitude of the voltage signal is chosen as 2mV and the frequency range is between 10 mHz to 100 Hz. The frequency range is selected on the basis of it being significant when considering an automotive drive cycle [10]. Based on these values, the EIS300 Software then calculates and applies an AC current followed by measuring the AC voltage. As the impedance varies over frequency, the amplitude of the AC current is continually regulated so that the AC voltage does not extend beyond the linear, non-destructive range of the cell.

5.2 Procedure

The general procedure involved during the tests using the Gamry equipment involved studying how the cells behaviour over different SOCs at a particular temperature. The temperature is then changed and then the same procedure is repeated, according to the parameters stated in Table 5.2. Since the cells being tested were highly sensitive to temperature, it is necessary that the temperature is maintained constant throughout the test. In order to accommodate for this, all tests were performed inside a Climate Chamber and additionally four NTC temperature sensors were used to monitor cell temperature at its tabs and on its body. The flowchart in Figure 5.1 briefly summarises the procedure followed during EIS measurements.

Table 5.2: List of parameter variations on EIS tests

Parameter of interest	Test range	Other variables
State of Charge(SoC)	0 to 100 %	constant T, I=0.5 mA
Temperature	-10 to 48 °C	0 to 100 % SOC, I=0.5 mA

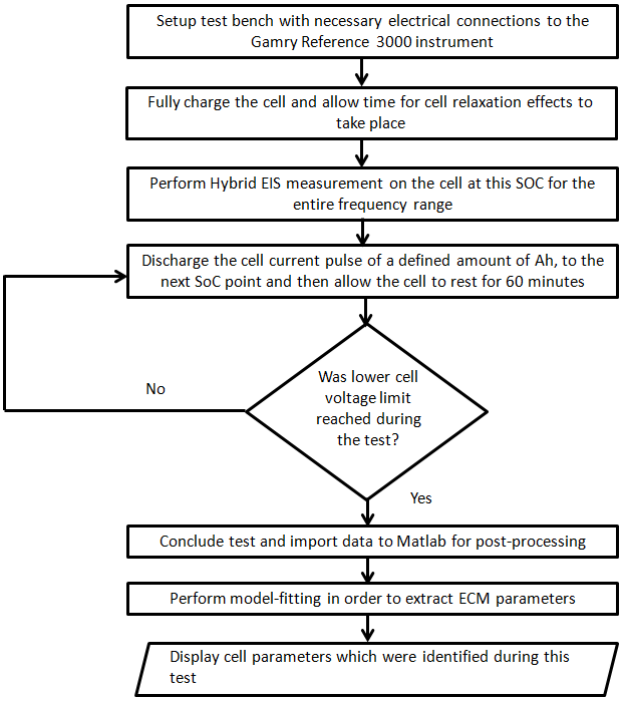

Figure 5.1: EIS overall test procedure

5.3 Measurements

5.3.1 OCV curve determination

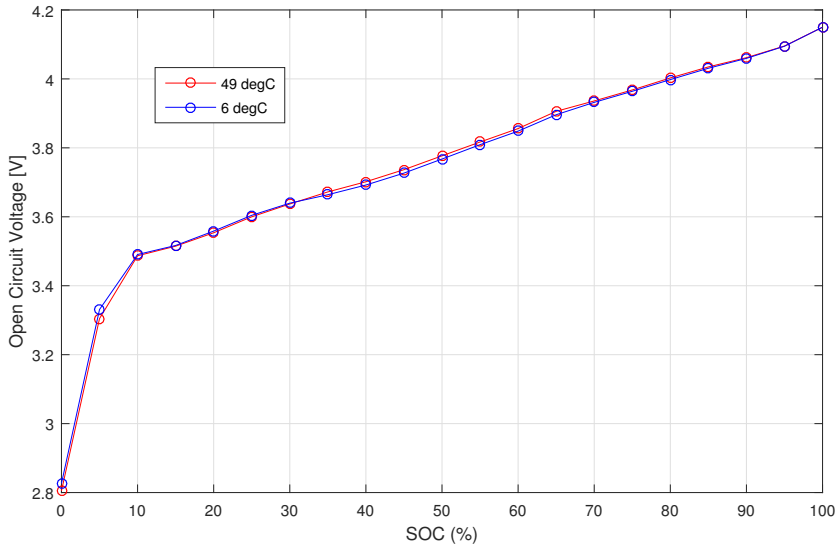

Figure 5.2: OCV vs SOC at two extreme temperatures for cell A

Since cell parameters tend to show strong dependency on its operating SOC point, it is of utmost importance to experimentally determine the OCV characteristics for every cell which is analysed using this small signal method. In order

to accomplish this, the approach suggested by the author of [13] is followed. This procedure involves charging and discharging the cell at a constant current and temperature, until and even a little beyond the operating voltage limits of the cell. During discharging, the cell terminal voltage can be represented as

$$y_1 = OCV(SOC) - R_{discharge}i \tag{5.1}$$

and correspondingly during charging it can be represented as

$$y_2 = OCV(SOC) + R_{charge}i. \tag{5.2}$$

From this, it is evident that the OCV can be determined as a function of SOC by adding (5.1) and (5.2) and taking their average. This would of course be assuming that the charging and discharging resistance to be the same. This point is earlier discussed in Section 2.3.2 and so it can be concluded that the inaccuracy involved here is quite small. Figure 5.2 shows a typical result obtained from this test and depicts the fact that even though OCV shows varies with SOC, it doesn't show too much variation at different temperatures within this range.

5.3.2 Impedance behaviour over SoC range

Figure 5.3 shows the EIS spectrum over the operating SOC window of cells A and C. It can be seen that both cells exhibit a similar EIS spectrum, which only differs in magnitude of impedance. It is evident that even though R_o is constant over all SOC points, R_{ct} varies greatly, and drastically increases at the end of the SOC window. Similar results were observed and reported in [1]. This phenomenon can be attributed to that fact that the graphite anode shrinks in size at low SOCs, thus making de-intercalation much harder[15].

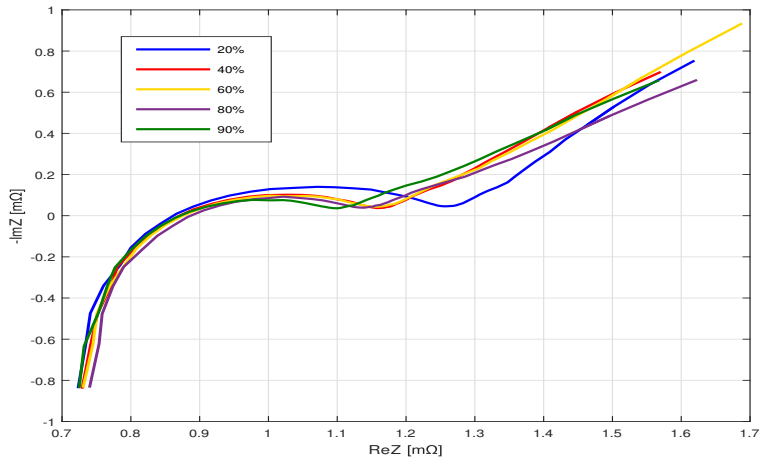

(a) Cell A

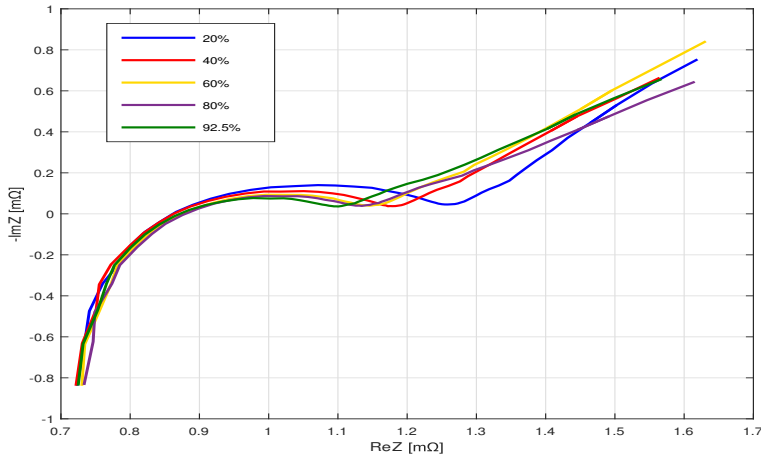

(b) Cell C

Figure 5.3: Impedance measurements at different points over the SOC window for Cell A and Cell C at 24 °C

5.3.3 Impedance behaviour over temperature range

Figure 5.4 shows that the EIS spectrum is quite similar even at different temperatures even though the magnitudes of the impedances differ greatly. It is evident that the ohmic resistance R_o of all three decreases with increase in temperature and this result agrees with similar work done in [1] and [21]. The value of the charge transfer resistance R_{ct} is also seen to significantly decrease with increase in temperature. The authors of [1] attribute this behaviour to have an exponential dependence on temperature according to the Arrhenius equation. Notably it can be seen that even though cell A and B belong to the same chemistry family and have very close values of R_{ct} at 24 °C, these values differ significantly at lower temperatures and this may be due to the presence of additives in the electrodes of either of the cells. It can be stated that an accuracy of ± 0.5°C is achieved in temperature measurement in this method.

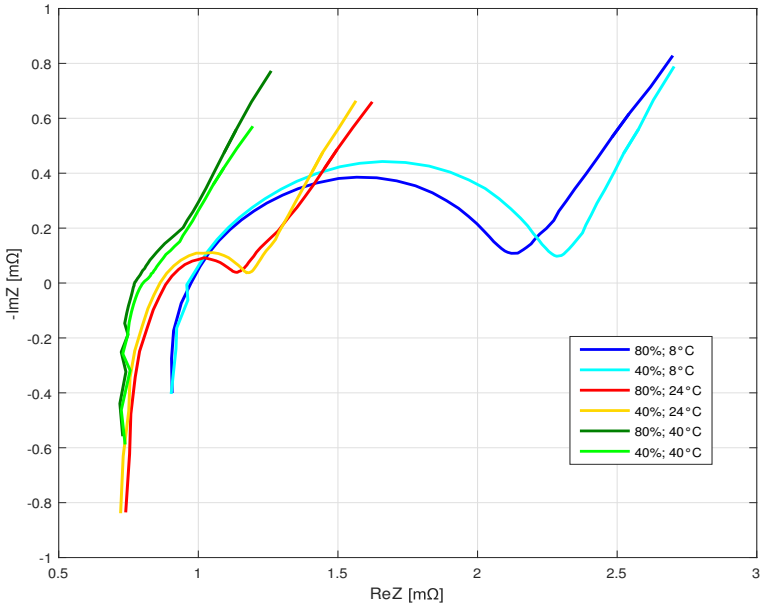

(a) Cell A

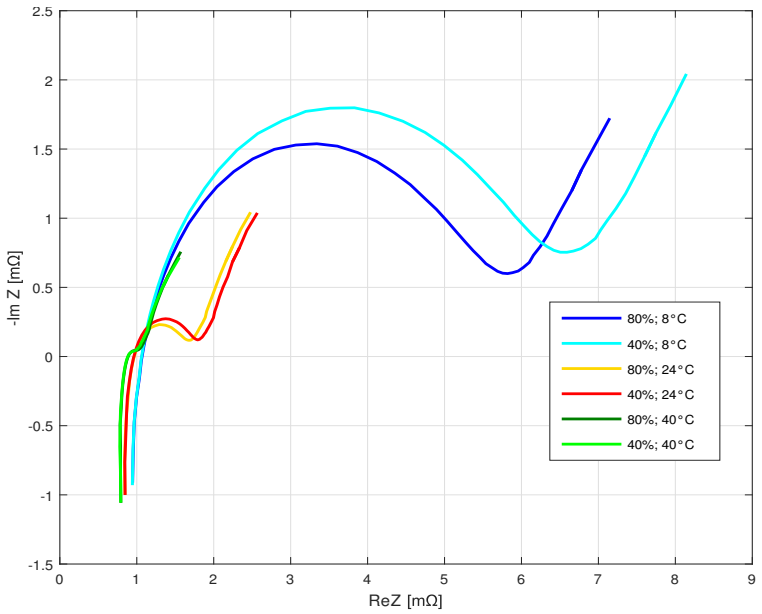

(b) Cell C

Figure 5.4: Measurements showing the behaviour of cells A and C at two specific SOC points and three operating temperatures

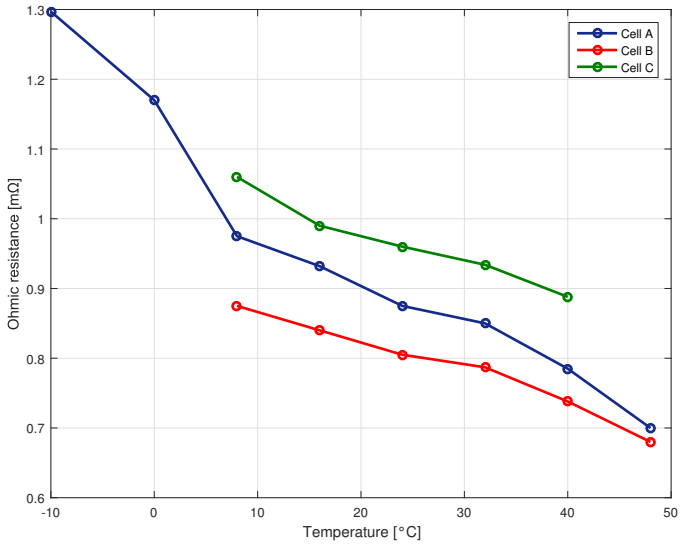

Figure 5.5: Behaviour of the ohmic resistance of cell A,B and C over temperature

The points in Figure 5.5 were plotted by extracting the point at which the EIS measurements of all the cells at several temperatures intersect the real axis. This point was found to be always independent of SOC. It can be used to study the behaviour of the R_o over a wide range of temperatures.

Chapter 6

Model fitting: Large signal

6.1 2 RC model fit

6.1.1 Algorithm

As described in Section 4.2.1, the voltage responses from the cell at each selected SOC point now needs to be processed in order to extract the cell's ECM parameters from it. In order to perform this task, the Fit tool available in Matlab is used.

$$y_{fit} = a_0 + a_1 e^{b_1 x} + a_2 e^{b_2 x} \tag{6.1}$$

is the expression which is fed into Fit function along with the cell voltage and time data. This expression was obtained in according with (2.1). Here a_0,a_1 and a_2 represent the respective steady state voltage drops over the resistances R_0,R_1 and R_2 respectively, while b_1 and b_2 represent the negative reciprocal of the quick and slow time constants. Since the Fit tool works using numerical optimisation methods, it is necessary to set initial values for the expected time constants, along with suitable upper and lower boundaries for them. This can be done by tuning the values of the variables b_1 and b_2.

6.1.2 Parameter identification

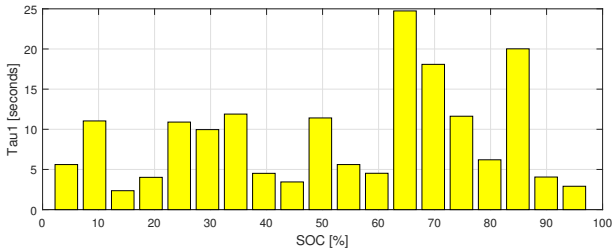

(a) Time constant of R_1C_1 :-1/b1

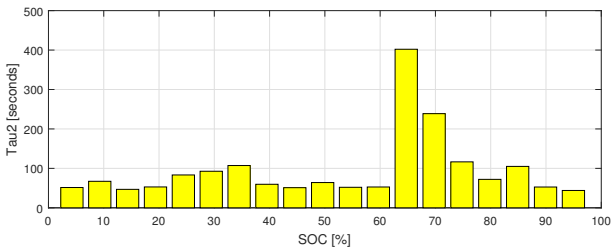

(b) Time constant of R_2C_2 :-1/b2

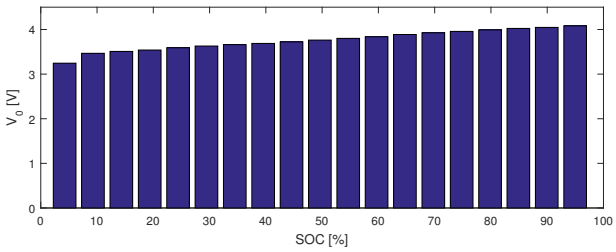

(c) Open circuit voltage:a_0

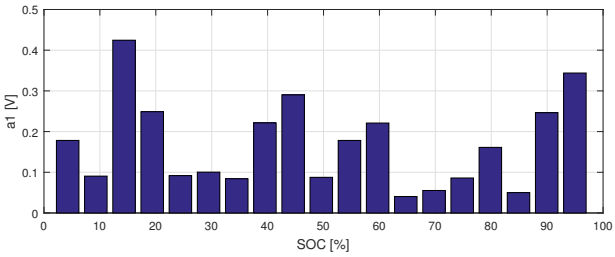

(d) Voltage drop over R_1:a_1

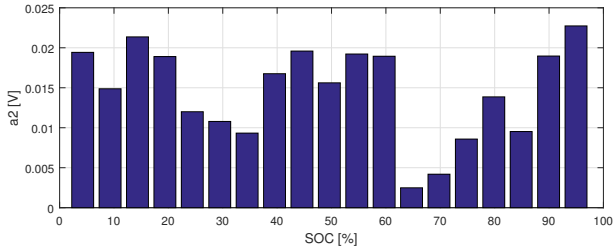

(e) Voltage drop over R_2:a_2

Figure 6.1: Typical time constant and voltage drop values obtained from curve fitting measurement done at 24 °C with 2C pulses

Figure 6.1 shows a typical graphical result which is obtained after application of the curve fitting tool. Each parameter required to solve (6.1) is represented as a function of SOC. However this is only an intermediate step in the process for ECM parameter identification. By utilising the values of the variables from the curve fit, the parameters of the DP model are calculated.

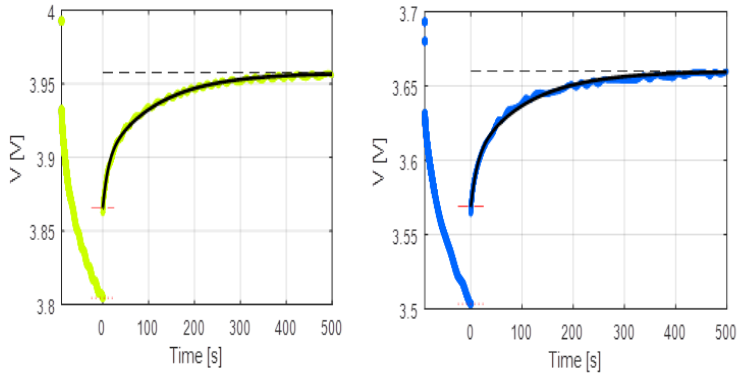

(a) Verification at two SOC points using measured cell relaxation and the simulated response

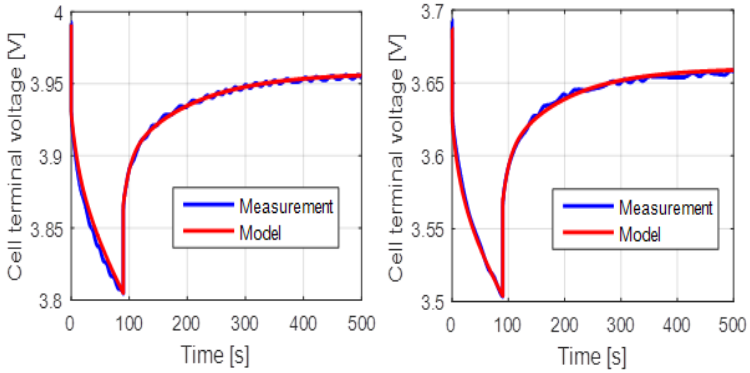

(b) Verification at two SOC points using measured cell voltage and the simulated response during complete current pulse

Figure 6.2: Output from Curve fitting

The values for the parameters shown in Figure 6.1, together with other values which were measured during the tests such as current pulse magnitude and pulse duration are then used to determine the values of R_0,R_1,R_2,C_1 and C_2 as functions of SOC. The values for the parameters obtained are then used as functions of SOC to populate a look-up table based Simulink/Simscape model of the cell. In order to verify that the parameter identification was executed properly, the simulation model is run with the same current pulse and with the cell at the same SOC point, and its voltage response is obtained. It is then visually compared with output obtained from the actual measurement as shown in Figure 6.2a. As another step for verification, the result of the entire voltage response including current injection and interruption of the simulation model is compared with that of the actual measurements as shown in Figure 6.2b.

6.2 R10 value based simulation

The R10 value of a cell is quite popularly used by battery users for simple cell modelling. Since the resistance of a Li ion cell varies as a function of time, this

value typically represents the cell resistance at time t=10 seconds. This however assumes that the cell was completely at rest at time t=0. When used instead of R_0 in a Rint model as in Figure 2.2, it would yield more accurate results. Once a DP model has been developed, this value can be simply estimated by calculating the ECM's resistance at 10 seconds.

Chapter 7

Model fitting: Small signal

7.1 6 RC model fit

The RC network based models described in Section 3.3.2 are parametrised in the frequency domain in accordance with the corresponding EIS measurements obtained at different SOC points and temperatures. In order to obtain a suitable fit between the simulated and measurement data, numeric optimisation was used. The method of approach involved using the Fminsearch function in Matlab to minimise the error between the measured EIS data and the output generated by a transfer function based model. The transfer function was developed on the basis of the model described in Section 3.3.2 and is mathematically represented as

$$H = R_0 + Ls + \frac{R_1}{R_1C_1s+1} + \frac{R_2}{R_2C_2s+1} + \frac{R_3}{R_3C_3s+1} + \frac{R_4}{R_4C_4s+1} + \frac{R_5}{R_5C_5s+1} + \frac{R_6}{R_6C_6s+1} \tag{7.1}$$

.

The Fminsearch algorithm basically requires an initial value for the parameters which are to be optimised, and after which it optimises the parameters of (7.1) in order to minimise the difference towards the measured data at a particular frequency. The initial values are carefully chosen so that 3 RC networks are used to represent each part of the EIS spectrum which would otherwise have been represented by a CPE. In order to quantify the fit obtained, the parameter Square of Sum of Errors(SSE) was used. Figure 7.1 shows the performance of this model over a wide range of SOC and temperatures.

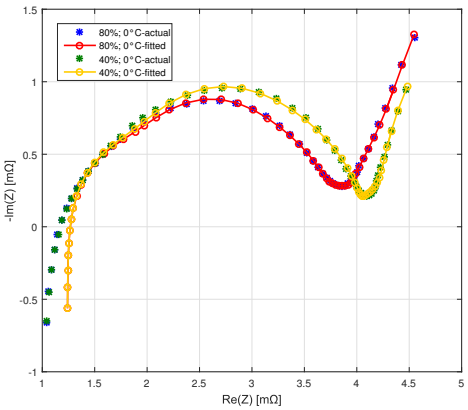

(a) Model fit for measurements at 0 °C

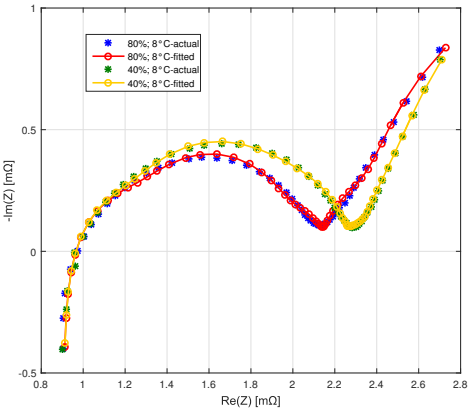

(b) Model fit for measurements at 8 °C

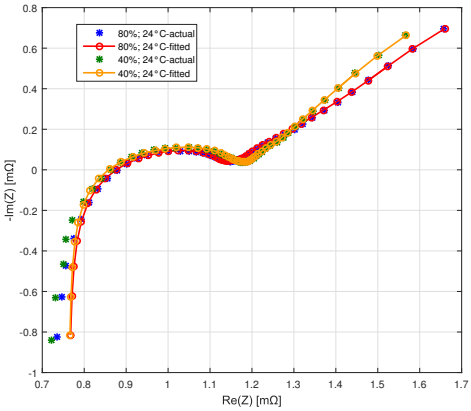

(c) Model fit for measurements at 24 °C

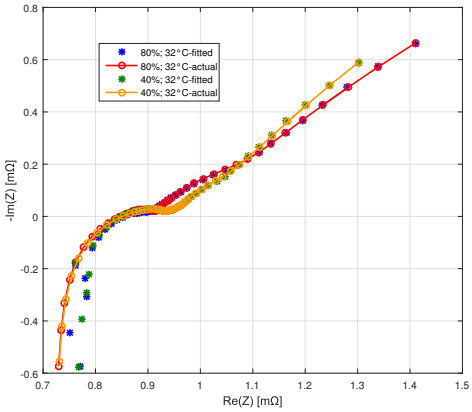

(d) Model fit for measurements at 32 °C

Figure 7.1: 6-RC based Model fit at two specific SOC points for different operating temperatures for cell A

7.2 2 RC model fit

A similar procedure to what was described above was followed here, with the exception that since much lesser number of elements were used, the initial values given to these two RC networks had to be so that they would try to replicate the diffusion part, which is commonly represented by a Warburg circuit element, thereby neglecting the higher frequencies. In order to make the optimisation algorithm focus more on the lower frequency part where the cell's impedance is higher, the error function is squared, so that algorithm now has not to minimise simply the error, but rather the square of it. Since EIS tests are performed only down to a frequency of 10 mHz, it is not possible to fit RC networks with too large time constants. For this model, a fast RC link with a time constant of a couple of seconds, and a slow RC link having a time constant of around 40 seconds is deemed suitable. Figure 7.2 shows the performance of this model over a wide

range of SOC and temperatures.

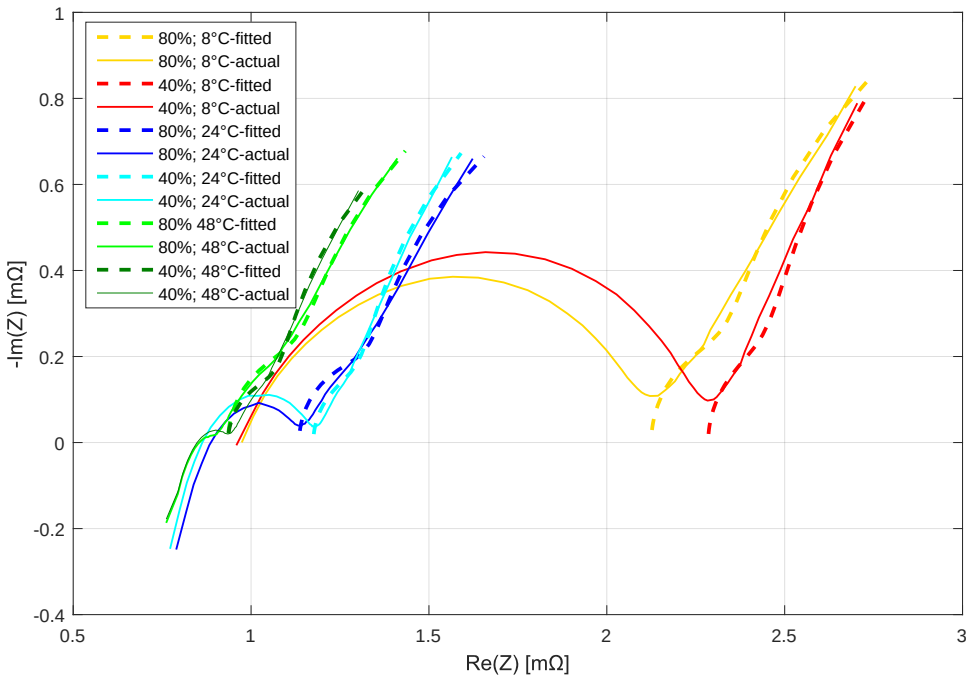

Figure 7.2: 2-RC based Model fit at two specific SOC points for different temperatures for cell A

Chapter 8

Comparison of all developed models

8.1 Cell behavioural trends captured by both methods

This chapter deals with the tests performed on cell B using both large and small signal methods. The results obtained from each method independently using the DP or 2RC link based model is compared with the other, in order to understand if both methods yield similar results. This is not a numerical comparison with respect to accuracy, but rather a comparison for the sake of getting a better understanding of how both models behave. The aspects regarding numerical accuracy of the models will be dealt with in the next chapter.

8.1.1 DC resistance behaviour over SOC and Temperature

Even though the tests following the two methods were performed at slightly different temperatures, it is evident that both methods are able to capture the characteristic trends exhibited by the cell. The only test which was performed at exactly the same temperature i.e. at 24 °C shows that the resistance magnitudes estimated through both methods are quite comparable. Notably, R_{ct} which is one of the two components of R_{DC} shows strong dependency on SOC as shown by other researchers[1][2]. Similarly, the decrease in R_{DC} at higher temperatures is due to the fact that both R_o and R_{ct} independently decrease with higher temperature.

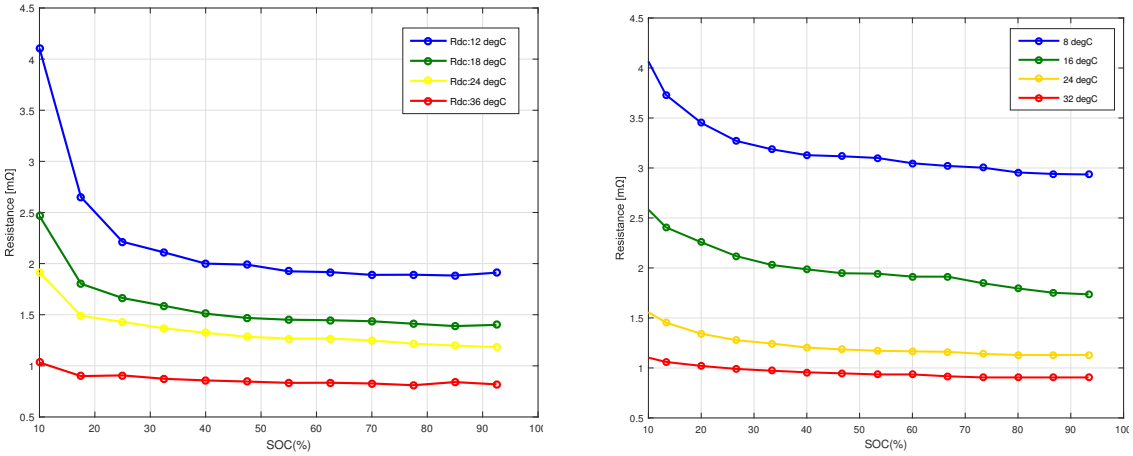

(a) Large signal method **(b)** Small signal method

Figure 8.1: DC Resistance of Cell B compared from both methods

8.1.2 Diffusion resistance behaviour over SOC and Temperature

The parameterisation of the R and C variables which represent the cell's diffusion behaviour is shown in the following collection of figures. The four other parameters required for the DP model are identified, but using the two different methods. Upon inspection of the Figures 8.2 and 8.3 which show the variations of the ECM parameters R_1,R_2,τ_1 and τ_2, it is evident that even though the results from the two methods may not be identical, the general trends captured are quite similar. Another reason for the non-identical results is since the time constants associated with the diffusion resistances are different for the two methods. Apparently, at higher temperatures, the resistance associated with diffusion is smaller and the reaction rates are faster. It is noteworthy that the phenomenon of the phase transition taking place at 70 % has also been captured by both methods.

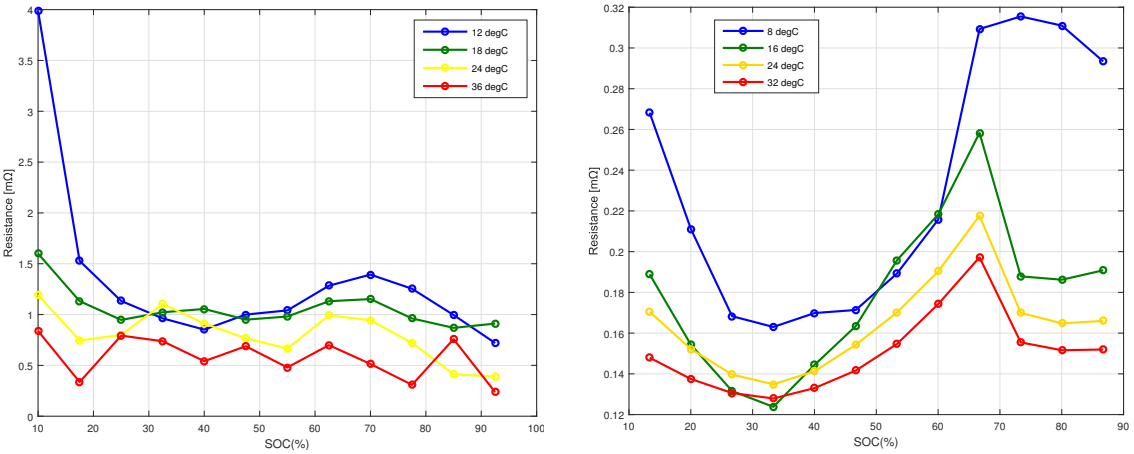

(a) Large signal method **(b)** Small signal method

Figure 8.2: Diffusion Resistance R1 for Cell B compared from both methods

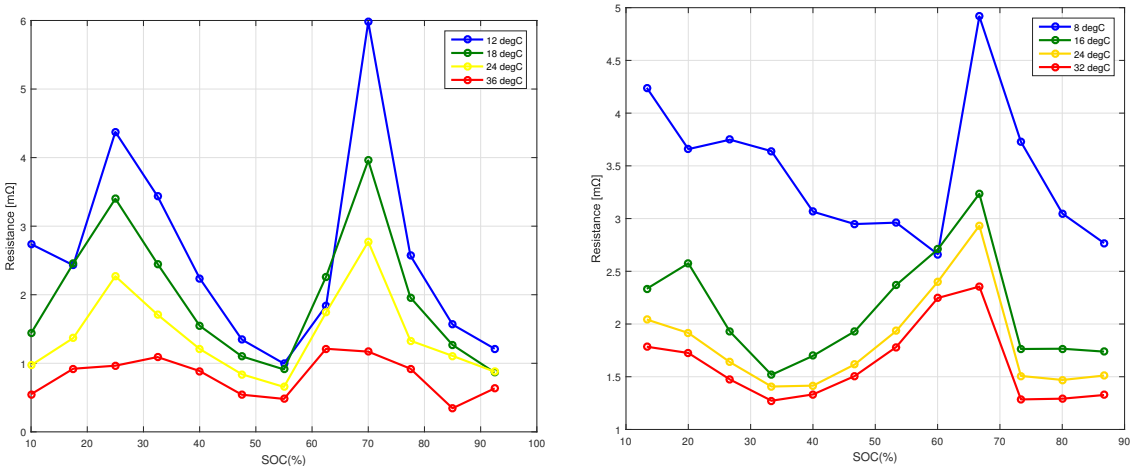

(a) Large signal method **(b)** Small signal method

Figure 8.3: Diffusion Resistance R2 for Cell B compared from both methods

8.1.3 Impedance dependence on C_{rate}

Since the Gamry EIS equipment is restricted in terms of its current loading capability, impedance characterisation with respect to different C-rates could only be done using the large signal method. The tests were performed on cells A and C, and it is evident that the impedance of the cell behaves differently depending upon the magnitude of current drawn from it.

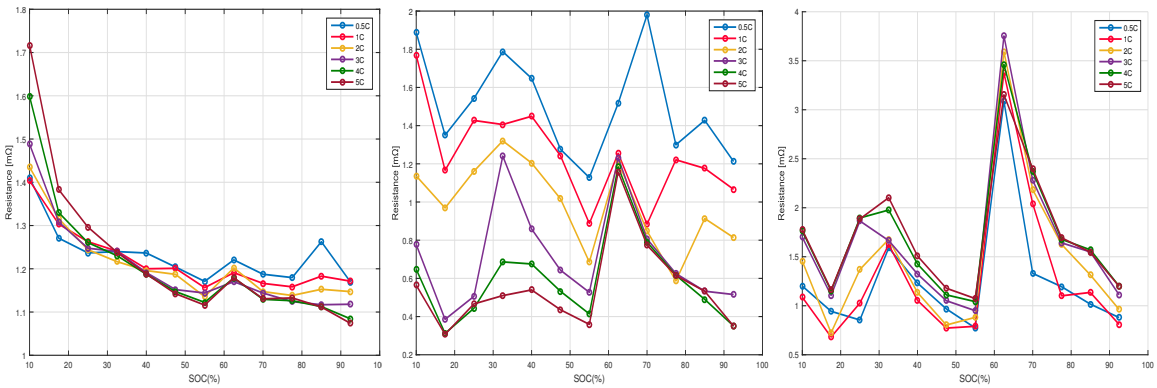

(a) Resistance R0 **(b)** Resistance R1 **(c)** Resistance R2

Figure 8.4: C_{rate} dependence of Cell A at constant temperature of 24 degrees C

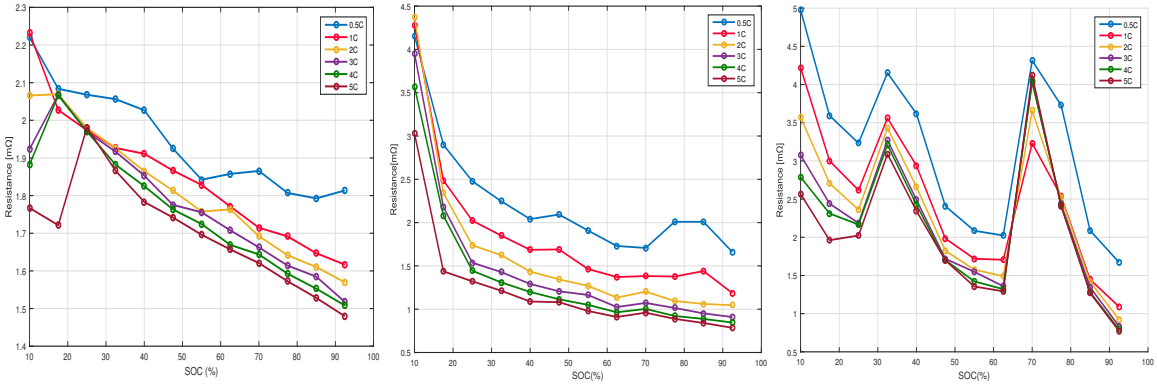

(a) Resistance R0 **(b)** Resistance R1 **(c)** Resistance R2

Figure 8.5: C_{rate} dependence of Cell C at constant temperature of 24 degrees C

Chapter 9

Validation of models

9.1 Development of simulation model

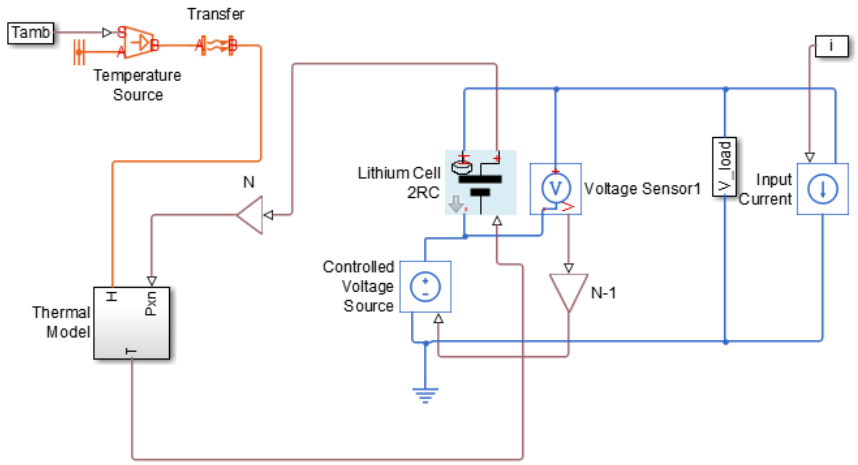

(a) Cell model

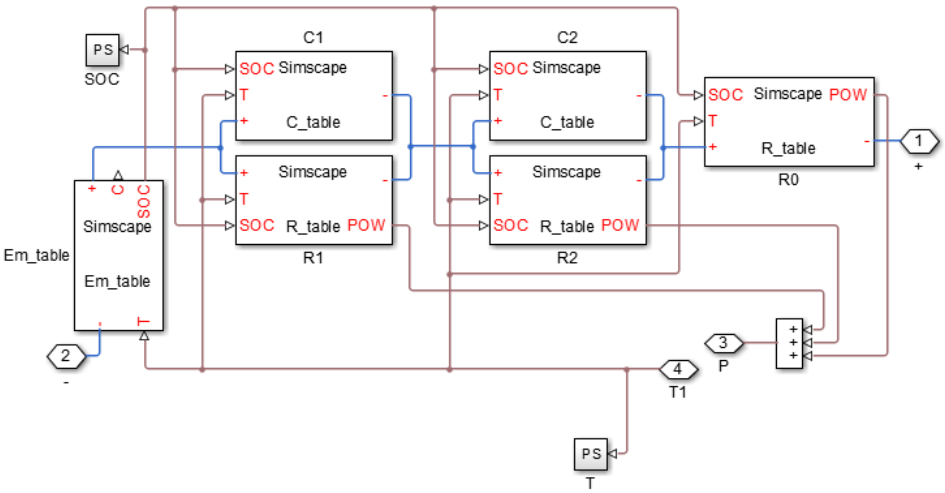

(b) Implementation of the Dual Polarisation ECM

Figure 9.1: Simulation model implemented in MATLAB Simulink/Simscape

MATLAB Simulnk/Simscape was chosen as a suitable environment to implement all the ECMs developed through the course of this work. The parameterised ECMs are fed into the cell simulation model shown in Figure 9.1, in the form of look-up tables which could have up to three dimensions. For instance, a parameter such as the R_{DC} requires a 2D LUT since it depends on SOC and temperature where as the OCV needs a 1D LUT. The Simulink environment allows easy application of simple current pulses as well as the use of complicated drive cycle inputs. Therefore, this model is quite robust and flexible to use.

9.2 Drive-cycle selection

In order to validate the models proposed, the Charge-Depleting Cycle Life Test Profile for the Minimum PHEV Battery will be used [10]. This dynamic drive cycle will be applied to two cells A and C which are of different chemistries and also at two temperatures, 24 and 10 °C respectively. Charge-Depleting Cycle life testing is performed using one of the Charge-Depleting Cycle Life Test Profiles wherein each cycle runs for 360 seconds. Cycle life testing is performed by repeating the test profile(s) until the Target Energy for the Charge-Depleting mode is reached. From then onwards the Charge-Sustaining mode is implemented implementing a test profile whose entire cycle keeps the battery SOC neutral.

9.3 Model evaluation by error comparison

Due to practical issues faced while applying the drive cycle on the cells, data pertaining to the Charge depletion mode alone is used for analysis and validation. Tables 9.1 and 9.2 show the Root Mean Square Error(RMSE) value for the validation test performed on the two cells A and C at 24°C. It can be seen that the comprehensive 6 RC performs poorly in comparison to the 2 RC models. Even though the performance of the 2RC models obtained from the large and small signal methods are different, they are produce satisfactory results. The difference between the parameters obtained from the two different methods could be due to the effect that the C-rate has on the cell impedance value as was shown previous in Section 8.1.3 and by the authors of [1]. It is seen that the performance of a model which simply uses the R10 value, which is estimated by choosing the real part of the impedance measured through EIS at a frequency of 0.1 Hz, is quite poor. It is noteworthy that the maximum error corresponding to such a model is also very high and is thereby unsuitable for dynamic cell modelling.

Table 9.1: Validation setup and results at 24 °C for cell A

ECM	Method of parametrisation	MSE [mV]
6 RC	Small signal	29
2 RC	Small signal	20
2 RC	Large signal	12
R10	Small signal	55

Table 9.2: Validation setup and results at 24 °C for cell C

ECM	Method of parametrisation	MSE [mV]
6 RC	Small signal	34
2 RC	Small signal	30
2 RC	Large signal	34
R10	Small signal	60

Chapter 10

Derivation of pulse power limits

10.1 Pulse power characterisation

The availability of a comprehensive ECM of a Li ion cell such as the DP model facilitates the accurate estimation of the pulse power capability of a cell under various operating conditions. If a comprehensive ECM such as the DP model was not developed for the cells under this study, the results found in this chapter would not have been possible. As mentioned previously , the value of maximum current chosen for pulse power characterisation is restricted to the maximum value permitted by the cell manufacturer. In order to characterise the pulse power that a cell can deliver for certain time intervals, an accurate estimate of its impedance behaviour is required. This is achieved using the DP ECM, by which accurate estimate of the cell's terminal voltage can be accomplished.

The pulse power limits depicted by Figures 10.1 and 10.2 were results obtained through the Simulation model which was earlier described in Section 9.1. The model consists of a battery comprising of 90 cells of type Cell B in series. A constant current load which draws a current equal to the maximum current capability of the cell was used in the model for the respective time interval of the pulse. The product of the battery terminal voltage and current was thus calculated as the power delivered by the battery.

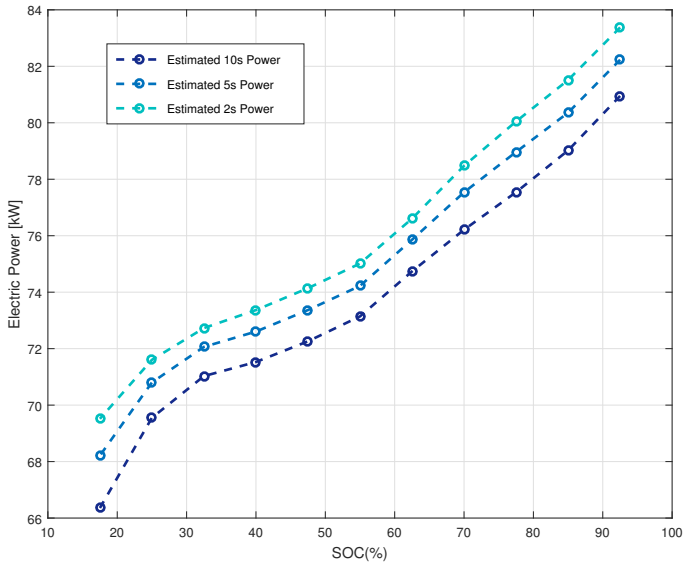

Figure 10.1: Pulse power capability with different pulse durations for battery containing cell B at 24 °C

Since the resistance of a cell is a function of time, the power capability shown in Figure can be expected. As discussed in Section 8.1.2, since diffusion effects take longer time to act, the resistance of a cell which has been at rest, is initially small, and then gradually increases. This enables the cell to deliver a higher magnitude of power for very short bursts of time.

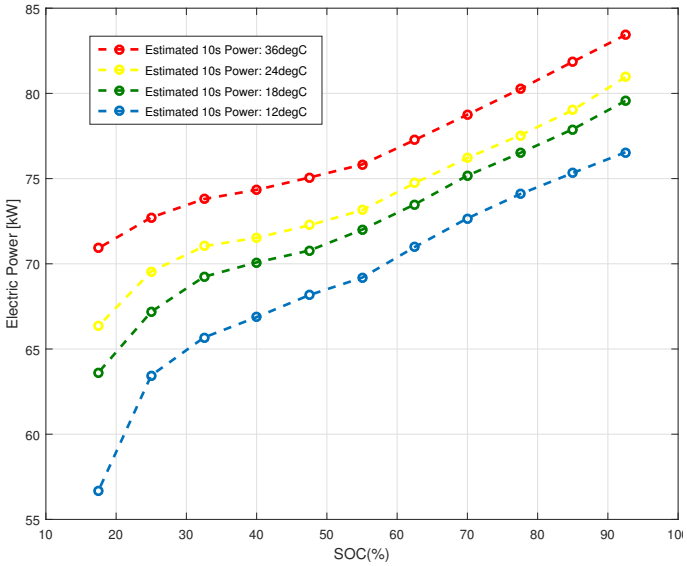

Figure 10.2: Pulse power capability over temperature for battery containing cell B

The trend in Figure 10.2 can again be explained as in Section 8.1, being due the reduction in the cell's DC resistance and also subsequent decrease of the diffusion resistance. Therefore it can be inferred that the pulse power capability of a cell in-

creases at higher temperatures. On the other hand, it also significantly decreases at lower temperatures due to the increase in the resistance.

Chapter 11

Conclusions

This work was aimed at quantifying the pulse power capability of a Li-ion cell under various operating conditions. In order to achieve this, it was necessary to develop a dynamic ECM with sufficient number of RC links to represent the behaviour of a Li-ion cell. In order to parameterise the developed model, the two methods, namely Current Interruption and EIS were unified and used in an unique manner. The results obtained through both methods were replicated using the Dual Polarisation ECM. Even though the two methods were significantly different, this work was able to unify the results of the two methods through the suitable application of the DP model. Further, the effectiveness of this model in terms of its accuracy was validated through testing it with a vehicle drive cycle. Upon comparing the results of the validation cycle, a RMSE value of close 30 mV was found when comparing actual measurement and simulation results. By the application of the parametrised ECM, the pulse power capability of a cell was characterised and quantified.

11.1 Future work

The pulse power available from a cell under different operating conditions was quantified in this thesis. Further work needs to be done in order to implement an algorithm in a vehicle by which the pulse power limits of a battery can be dynamically varied. Moreover, the scope of this thesis was limited to new cycles which were at their Beginning of Life and so it would be important to perform similar experiments on cells at various stages of aging, and analyse the decrease in pulse power capability of the cell. EIS was found to be a very suitable method for analysing the cell impedance behaviour, and its application could be further extended into using it for online impedance diagnostics so that pulse power limits of a cell can be adjusted over its lifetime in a vehicle.

Bibliography

[1] W. Waag, S. Käbitz, and D. U. Sauer, "Experimental investigation of the lithium-ion battery impedance characteristic at various conditions and aging states and its influence on the application," *Applied Energy*, vol. 102, pp. 885–897, 2013.

[2] B. Ratnakumar, M. Smart, L. Whitcanack, and R. Ewell, "The impedance characteristics of mars exploration rover li-ion batteries," *Journal of power sources*, vol. 159, no. 2, pp. 1428–1439, 2006.

[3] D. Andre, M. Meiler, K. Steiner, H. Walz, T. Soczka-Guth, and D. Sauer, "Characterization of high-power lithium-ion batteries by electrochemical impedance spectroscopy. ii: Modelling," *Journal of Power Sources*, vol. 196, no. 12, pp. 5349–5356, 2011.

[4] L. Lu, X. Han, J. Li, J. Hua, and M. Ouyang, "A review on the key issues for lithium-ion battery management in electric vehicles," *Journal of power sources*, vol. 226, pp. 272–288, 2013.

[5] J. Groot, "State-of-health estimation of li-ion batteries: Cycle life test methods," 2012.

[6] T. M. Bandhauer, S. Garimella, and T. F. Fuller, "A critical review of thermal issues in lithium-ion batteries," *Journal of the Electrochemical Society*, vol. 158, no. 3, pp. R1–R25, 2011.

[7] S. S. Choi and H. S. Lim, "Factors that affect cycle-life and possible degradation mechanisms of a li-ion cell based on licoo 2," *Journal of Power Sources*, vol. 111, no. 1, pp. 130–136, 2002.

[8] Y. Olofsson, J. Groot, T. Katrasnik, and G. Tavcar, "Impedance spectroscopy characterisation of automotive nmc/graphite li-ion cells aged with realistic phev load profile," in *Electric Vehicle Conference (IEVC), 2014 IEEE International*. IEEE, 2014, pp. 1–6.

[9] J. Gomez, R. Nelson, E. E. Kalu, M. H. Weatherspoon, and J. P. Zheng, "Equivalent circuit model parameters of a high-power li-ion battery: Thermal and state of charge effects," *Journal of Power Sources*, vol. 196, no. 10, pp. 4826–4831, 2011.

[10] A. S. for Energy Efficiency and R. E. E. I. O. Office, "Idaho national engineering and environmental laboratory," *Battery Test Manual for Plug-In Hybrid Electric Vehicles*, 2010.

[11] S. Buller, *Impedance Based Simulation Models for Energy Storage Devices in Advanced Automotive Power Systems*. Shaker, 2002.

[12] T. HURIA, "Rechargeable lithium battery energy storage systems for vehicular applications," 2012.

[13] A. A. Hussein, "Experimental modeling and analysis of lithium-ion battery temperature dependence," in *Applied Power Electronics Conference and Exposition (APEC), 2015 IEEE*. IEEE, 2015, pp. 1084–1088.

[14] A. Barai, G. H. Chouchelamane, Y. Guo, A. McGordon, and P. Jennings, "A study on the impact of lithium-ion cell relaxation on electrochemical impedance spectroscopy," *Journal of Power Sources*, vol. 280, pp. 74–80, 2015.

[15] J. Illig, *Physically based Impedance Modelling of Lithium-Ion Cells*. KIT Scientific Publishing, 2014, vol. 27.

[16] H.-G. Schweiger, O. Obeidi, O. Komesker, A. Raschke, M. Schiemann, C. Zehner, M. Gehnen, M. Keller, and P. Birke, "Comparison of several methods for determining the internal resistance of lithium ion cells," *Sensors*, vol. 10, no. 6, pp. 5604–5625, 2010.

[17] Y. Li, B. Zhang, M. Chen, D. Yang, and J. Liu, "Investigation of the internal resistance in lifepo 4 cells for battery energy storage system," in *Industrial Electronics and Applications (ICIEA), 2014 IEEE 9th Conference on*. IEEE, 2014, pp. 1596–1600.

[18] J. V. Barreras, E. Schaltz, S. J. Andreasen, and T. Minko, "Datasheet-based modeling of li-ion batteries," in *Vehicle Power and Propulsion Conference (VPPC), 2012 IEEE*. IEEE, 2012, pp. 830–835.

[19] A. Rahmoun and H. Biechl, "Modelling of li-ion batteries using equivalent circuit diagrams," *Electrical review, ISSN*, pp. 0033–2097, 2012.

[20] R. Jackey, M. Saginaw, P. Sanghvi, J. Gazzarri, T. Huria, and M. Ceraolo, "Battery model parameter estimation using a layered technique: An example using a lithium iron phosphate cell," *SAE Technical Paper*, pp. 01–1547, 2013.

[21] D. Andre, M. Meiler, K. Steiner, C. Wimmer, T. Soczka-Guth, and D. Sauer, "Characterization of high-power lithium-ion batteries by electrochemical impedance spectroscopy. i. experimental investigation," *Journal of Power Sources*, vol. 196, no. 12, pp. 5334–5341, 2011.

[22] H. He, R. Xiong, and J. Fan, "Evaluation of lithium-ion battery equivalent circuit models for state of charge estimation by an experimental approach," *Energies*, vol. 4, no. 4, pp. 582–598, 2011.

[23] Gamry application note. [Online]. Available: http://www.gamry.com/application-notes/EIS/basics-of-electrochemical-impedance-spectroscopy/

[24] A. Narula, "Modeling of ageing of lithium- ion battery at low temperatures," 2012.

[25] P. Verma, P. Maire, and P. Novák, "A review of the features and analyses of the solid electrolyte interphase in li-ion batteries," *Electrochimica Acta*, vol. 55, no. 22, pp. 6332–6341, 2010.

[26] M. A. Roscher, J. Vetter, and D. U. Sauer, "Cathode material influence on the power capability and utilizable capacity of next generation lithium-ion batteries," *Journal of Power Sources*, vol. 195, no. 12, pp. 3922–3927, 2010.

[27] Gamry reference manual. [Online]. Available: http://www.gamry.com/assets/Uploads/Reference-3000-Operators-Manual.pdf